

Mechanical Properties of Vapor–Liquid–Solid Synthesized Silicon Nanowires

Yong Zhu,^{*,†} Feng Xu,[†] Qingquan Qin,[†] Wayne Y. Fung,[‡] and Wei Lu[‡]

Department of Mechanical and Aerospace Engineering, North Carolina State University, Raleigh, North Carolina 27695, and Department of Electrical Engineering and Computer Science, The University of Michigan, Ann Arbor, Michigan 48109

Received July 4, 2009; Revised Manuscript Received August 7, 2009

ABSTRACT

The Young's modulus and fracture strength of silicon nanowires with diameters between 15 and 60 nm and lengths between 1.5 and 4.3 μm were measured. The nanowires, grown by the vapor–liquid–solid process, were subjected to tensile tests in situ inside a scanning electron microscope. The Young's modulus decreased while the fracture strength increased up to 12.2 GPa, as the nanowire diameter decreased. The fracture strength also increased with the decrease of the side surface area; the increase rate for the chemically synthesized silicon nanowires was found to be much higher than that for the microfabricated silicon thin films. Repeated loading and unloading during tensile tests demonstrated that the nanowires are linear elastic until fracture without appreciable plasticity.

Silicon (Si) nanowires (NWs) are one of the key building blocks for nanoelectronic and nanoelectromechanical devices.¹ They exhibit excellent mechanical,^{2,3} electrical,⁴ and optical⁵ properties, in addition to interesting multifunctional properties such as piezoresistivity⁶ and thermoelectricity.^{7–9} As such, Si NWs have been used in a broad range of applications including nanoelectronics,^{10–12} nanosensors,¹³ nanoresonators,¹⁴ light-emitting diodes,¹⁵ and thermoelectric energy scavengers.^{7,8} The operation and reliability of these nanodevices depend on the mechanical properties of Si NWs, which are expected to be different from their bulk counterparts due to their increasing surface-to-volume ratio.

Existing techniques for measuring the mechanics of individual NWs include observing the vibration (or resonance) of cantilevered NWs inside a transmission or scanning electron microscope (TEM/SEM),^{16–18} measuring the lateral bending of suspended NWs with an atomic force microscope (AFM),^{3,19–21} measuring uniaxial tension of suspended NWs in SEM or TEM,^{2,22–26} and nanoindentation of NWs on a substrate.²⁷ Available experimental results on Si NWs exhibit significant scatter including the following: (1) some reported a decrease in Young's modulus with decreasing size,^{2,9,24,28} while others showed an opposite trend;^{20,21} (2) the reported strength values of vapor–liquid–solid (VLS) grown Si NWs

ranged from 500 MPa to 12 GPa;^{3,28} (3) Han et al.² observed pronounced plastic deformation of Si NWs by in situ TEM tensile tests at room temperature, while Gordon et al.²¹ reported linear elastic behavior followed by brittle fracture using AFM bending tests.

Moreover the experimental data show large discrepancy with the simulation results.²⁹ For instance, the experimentally measured Young's moduli started deviating from the bulk value at diameters of about 200 nm;²⁸ conversely, computational studies using both density functional theory (DFT) and classical molecular dynamics (MD) indicated that the transition diameter for Young's modulus of Si NWs is less than 10 nm.^{30–32} The experimentally observed plasticity at room temperature occurred for Si NWs with diameter less than 60 nm, while MD simulations³³ predicted a similar brittle-to-ductile transition (BDT) for Si NWs with diameter smaller than 4 nm at room temperature. Apparently, there exists a substantial gap between experiments and simulations in the transition size in both the elastic and inelastic properties of Si NWs.

In this paper we report the quantitative stress–strain measurements of Si NWs using tensile tests for the first time. We present experimental results on Si NWs with diameters ranging from 15 to 60 nm. The NWs were synthesized using the VLS process. The tests were conducted using a nanomanipulator as the actuator and an AFM cantilever as the load sensor inside a SEM. It was observed that the Young's modulus decreased while fracture strength increased up to over 12 GPa, as the NW diameter decreased. The fracture

* To whom correspondence should be addressed. Phone: (919) 513-7735. Fax: (919) 515-7968. E-mail: yong_zhu@ncsu.edu.

[†] Department of Mechanical and Aerospace Engineering, North Carolina State University.

[‡] Department of Electrical Engineering and Computer Science, The University of Michigan.

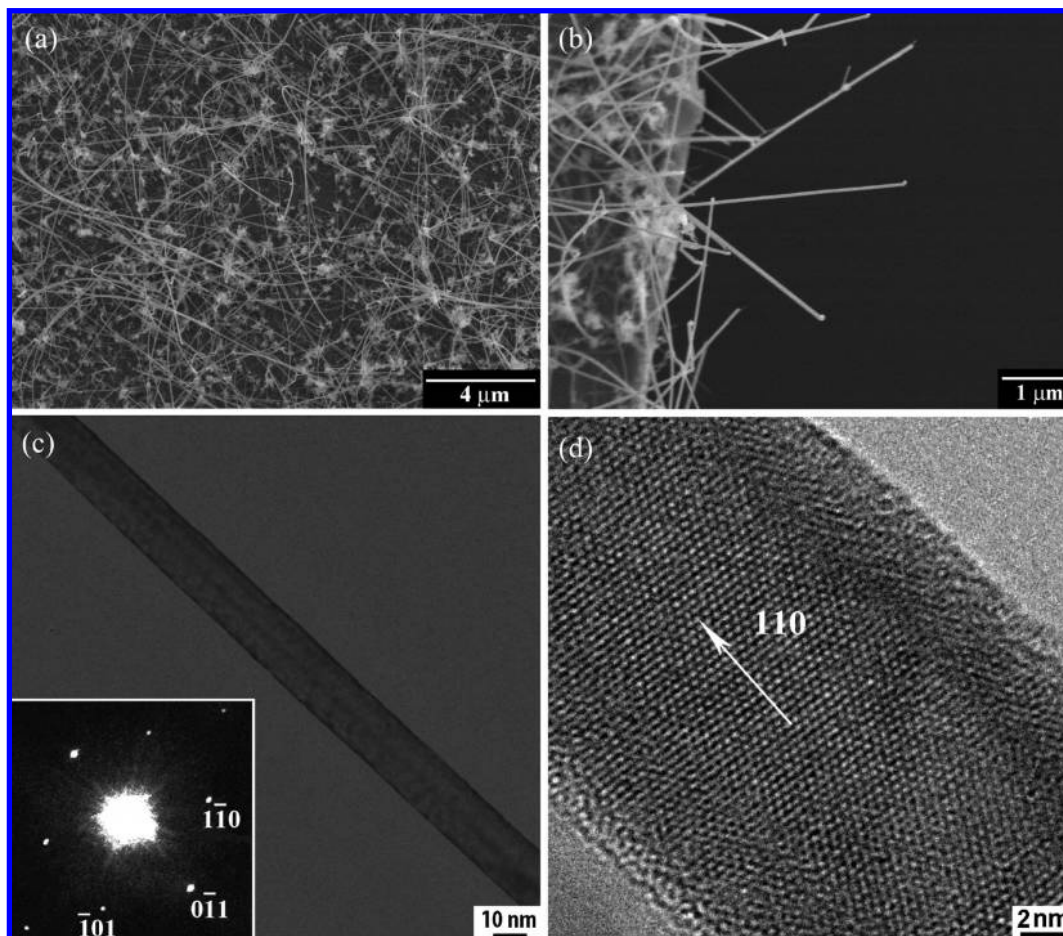


Figure 1. (a) Typical SEM image of the Si NWs grown from 50 nm diameter Au nanoparticles. (b) Enlarged SEM image of Si NWs protruding out from the edge of the substrate. (c) TEM image of a single Si NW. Inset of (b): The corresponding SAED pattern of the Si NW with zone axis along $[111]$. (d) HRTEM image of the NW.

strength also increased with the decrease of the side surface area. Repeated loading and unloading during tensile tests demonstrated that the NWs are linear elastic until fracture without appreciable plasticity.

Si NWs were synthesized by chemical vapor deposition (CVD) using gold nanoclusters as catalysts and silane (SiH_4) as a vapor-phase reactant, following the method developed by Wu et al.^{1,34} Gold nanoclusters with diameters ranging from 10 to 50 nm were deposited on Si substrates capped with a 600 nm thick layer of thermal silicon dioxide. The substrates were placed in a quartz tube furnace (EasyTube 3000, First Nano). After a 30 min purge in H_2 ambient at 50 Torr, VLS growth of nanowires was carried out at 480 °C, 15 Torr for 10 min with the flow of SiH_4 (20 sccm) and H_2 (200 sccm).

The Si NWs grown from Au nanoclusters were nearly monodisperse with diameters determined by the nanoclusters. Figure 1a shows an SEM image of Si NWs produced from 50 nm diameter Au nanoclusters. Figure 1b is an enlarged SEM image, displaying that some Si NWs protrude out from the edge of the Si wafer. These NWs can be easily manipulated for the experiments reported in this paper. Figure 1c shows the TEM image of a Si NW with diameter close to 20 nm. It can be seen that the NW is not only straight but also uniform in width along the growth direction. The

selected area electron diffraction (SAED) pattern in the inset of Figure 1c indicates that the NW growth direction is $\langle 110 \rangle$. Figure 1d is a high-resolution transmission electron microscopy (HRTEM) image, which indicates the single-crystal nature of the Si NWs and also confirms the growth direction of $\langle 110 \rangle$. Careful characterization of Si NWs synthesized using this method has shown that NWs with diameters larger than 20 nm grow primarily along the $\langle 111 \rangle$ direction, whereas the NWs with smaller diameter could have three growth directions: $\langle 110 \rangle$, $\langle 112 \rangle$, and $\langle 111 \rangle$.^{1,34} Furthermore, these Si NWs have little or no visible amorphous oxide on the NW surface (see Supporting Information).³⁴ It is believed that using H_2 as the carrier gas passivates the surface. Our Si NWs are different from many other Si NWs reported in the literature using either the CVD-VLS method²¹ or other methods such as thermal evaporation,^{2,35} where the Si NW surfaces are either covered with an at least 1–3 nm thick amorphous oxide or treated to be hydrogen terminated. The surface condition might play an important role in the mechanical property of Si NWs as will be discussed later.

The tension tests were performed inside an SEM (JEOL 6400F). A nanomanipulator (Klocke Nanotechnik, Germany) with 1 nm resolution and 1 cm travel range in three orthogonal directions was used to pick up protruding NWs from the Si wafer following the procedure developed by Zhu

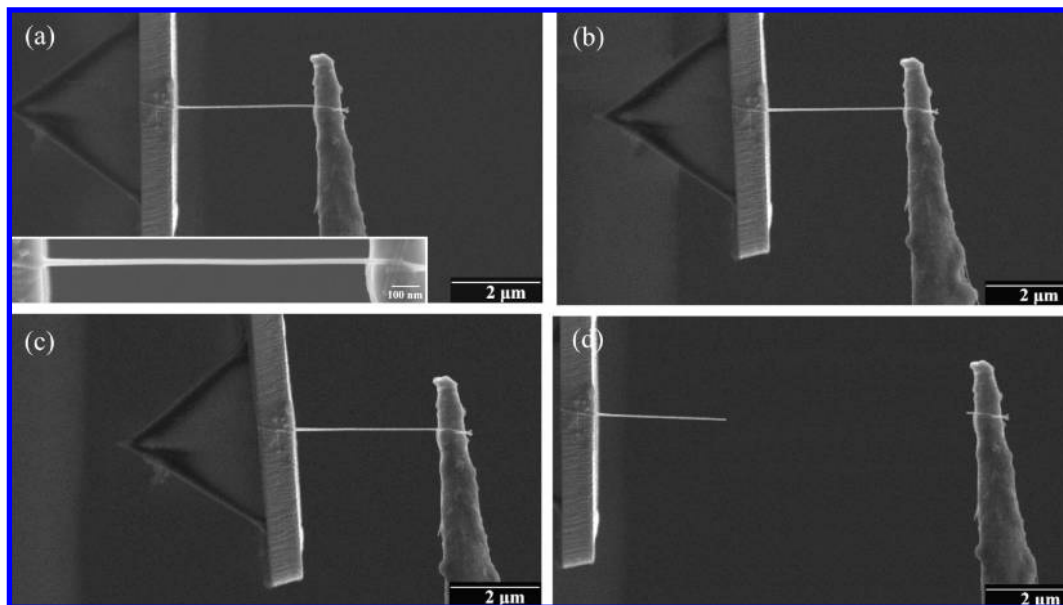


Figure 2. (a–c) A series of SEM images taken during the tensile test for a Si NW with diameter of 23 nm. Inset of (a): High resolution SEM image of the NW for strain measurements. (d) SEM image showing that fracture occurs on the NW when the load was applied to a certain value.

and Espinosa.³⁶ For tension tests, an AFM chip (ORC8-10, Veeco) with two silicon nitride cantilevers on each side was mounted on a sample holder. After a Si NW was clamped to the tungsten tip of the nanomanipulator using electron beam induced deposition (EBID) of carbonaceous materials in the SEM chamber, the NW was pulled away from the Si wafer, moved toward the AFM cantilever, and clamped on the side of the cantilever using the EBID again. Subsequently, the specimen was loaded and unloaded for a few cycles to investigate the elastic and possible inelastic properties. A series of SEM images were taken during the tensile process. Both force and elongation can be directly measured from the images. It is possible that a small torsion of the cantilever might occur under the applied tensile force as the specimen is clamped on the side of the cantilever. However, this error was found to be negligible according to the SEM images. Overall this tensile testing technique is similar to that developed by Yu et al.³⁷ but differs in that a sharp tungsten tip instead of an AFM tip is used for NW manipulation and actuation. The high aspect ratio of the tungsten tip is advantageous in picking up NWs. In addition, in our configuration, the nanomanipulator is mounted on the SEM flange and the sample is placed on the SEM sample stage. This allows all the degrees of freedom of the SEM sample stage.

The spring constant of the cantilever was calibrated using the Sader method.³⁸ According to his method, the spring constant of the AFM cantilever used in tension tests was measured as 0.70 ± 0.05 N/m. The cantilever deflection was measured in images with lower magnification, where a resolution of half pixel translated to 7.5 nm. Therefore the force resolution was 5.25 ± 0.38 nN. For NWs with diameters ranging from 15 to 60 nm, the stress resolution ranged from 29.7 to 1.8 MPa. The NW elongation was measured in images with a higher magnification (the image

possesses 2000×1600 pixels and a nanowire typically spans 1500–1800 pixels in length). Therefore, the strain resolution is about 0.03%.

Panels a–c of Figure 2 show a series of SEM images taken during the tensile test for a NW with diameter of 23 nm. Figure 2a is the image prior to loading. Panels b and c of Figure 2 show the NW under the strain of 0.023 and 0.062, respectively. The loads on the NW were calculated from the cantilever deflections, which were obtained in the images with reference to a stationary feature at the left of the image. The stationary feature was the neighboring cantilever on the same chip and was out of focus in the SEM images due to the difference in focal depth. The force and elongation of the NW were measured based on these images and then converted to stress and strain. Additional SEM images with high magnification were taken at each loading step, as shown in the inset of Figure 2a, to increase the strain resolution. The NW was tested in a few loading and unloading cycles until fracture (Figure 2d).

Figure 3a shows the stress–strain response of this NW. The Young’s modulus was measured to be 166 GPa, which is lower than the bulk value of Si in the [111] direction (187 GPa).³⁹ It can be seen that the loading and unloading curves followed almost the same path showing a linear elastic behavior. No residual plastic deformation was observed when the NW was totally unloaded. This observation is corroborated with the enlarged image of the broken NW shown in Figure 3b. The broken end seems flat and no noticeable diameter reduction or necking. No NW slippage was observed at both ends, indicating the carbon deposition clamp was strong enough for testing Si NWs with diameters up to 60 nm (see Supporting Information). Tension tests of all the NWs at different diameters were conducted following the same procedure with multiple loading/unloading cycles and all the NWs showed linear elastic behavior.

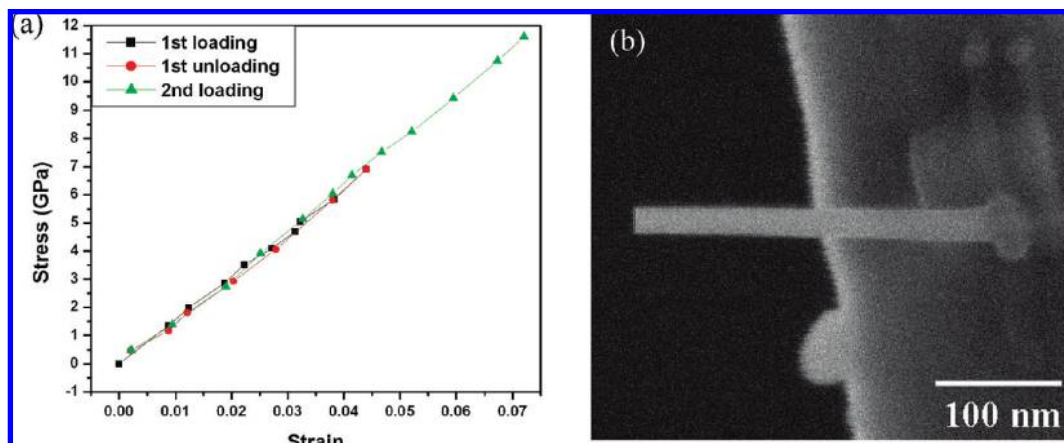


Figure 3. (a) A typical stress–strain response of the specimens with diameter of 23 nm under repeated loading and unloading. (b) Enlarged SEM image of the broken end of the Si NW on the probe tip.

To study the size effects on the mechanical properties of Si NWs, a total 10 NWs with diameters ranging from 15 to 60 nm were tested. Figure 4a shows the measured Young’s moduli of all the tested NWs as a function of NW diameter. Dotted lines are theoretical values for Si in the directions specified.³⁹ It is evident that the Young’s modulus of Si NWs is almost constant, around the bulk value for the $\langle 111 \rangle$ orientation (187 GPa) when the diameters are larger than 30 nm. However, the softening trend is obvious for NWs with smaller diameters; the Young’s modulus decreases with the decreasing diameters. As discussed earlier, for NWs with diameters less than 20 nm, the growth direction could be $\langle 110 \rangle$, $\langle 112 \rangle$, or $\langle 111 \rangle$. The bulk Young’s moduli for $\langle 110 \rangle$ and $\langle 112 \rangle$ orientations are 169 GPa.³⁹ Therefore, the softening in the Young’s modulus of Si NWs is clear no matter what the growth direction is.

Multiscale simulations including continuum mechanics, molecular mechanics, and first principle calculations have been conducted to investigate the size effects in the elastic behavior of nanostructures. Several major mechanisms have been proposed including (1) surface effects (surface stress and surface elasticity),^{30,33,40–42} (2) nonlinear elastic response of the NW core,⁴³ and (3) specifically for NWs with an oxide layer such as Si NWs, increasing importance of the oxide shell following the simple core–shell model.^{19,21,44} In view that the modulus of silicon oxide is smaller than that of Si, Si NWs with reducing NW diameter but constant oxide layer possess smaller Young’s modulus. But for the Si NWs tested in our experiments, there is little or no visible amorphous oxide on the surface as evidenced in the HRTEM image.³⁴ So the contribution of the oxide layer to the Young’s modulus of Si NWs following the core–shell model is negligible. However, we cannot rule out the possibility that such a thin oxide layer might change the surface stress state, which might influence the Young’s modulus of Si NWs. According to the DFT calculations of $\langle 100 \rangle$ Si NWs conducted by Lee and Rudd,³⁰ the nonlinear bulk elasticity had a negligible effect on the Young’s modulus of Si NWs. Note that the simulated Si NWs were passivated by hydrogen and the passivation mitigated the surface stress of reconstructed surfaces. Therefore, the remaining and most likely mecha-

nism is the surface effects, which was found to strongly depend on the surface reconstruction. The surface reconstruction can lead to bond saturation, bond contraction or elongation, and loss of bonding neighbors.⁴¹ Direct comparisons between experiments and simulations for Si NWs with the same geometry and surface conditions could further elucidate the mechanisms for the observed size effects. It should be noted that our results are in good agreement with the multiscale resonance calculations that predicted elastic softening in $[100]$ Si NWs when the NW diameter dropped below 30 nm, although the crystalline orientations in two studies are different.⁴²

Panels b and c of Figure 4 show the fracture strain and fracture strength as functions of the NW diameters from the tension tests. It can be seen that the fracture strain increased from 2.7% to about 12% when the NW diameter decreased from 60 to 15 nm. Similarly, the fracture strength was found to increase from 5.1 GPa to slightly about 12.2 GPa when the NW diameter decreased from 60 to 15 nm. A strength of 12.2 GPa is the closest reported value to the theoretical strength of 15.2 and 18.8 GPa for Si along the $\langle 110 \rangle$ and $\langle 111 \rangle$ directions, respectively.⁴⁵ It is interesting to notice that the fracture strength dropped when the NW diameter is below 20 nm. This phenomenon may be related to the growth direction of the NWs, since the ideal strength of a material is related to its Young’s modulus. The NWs grown along $\langle 110 \rangle$ or $\langle 112 \rangle$ have Young’s moduli lower than those along the $\langle 111 \rangle$ direction;⁴⁵ therefore it is possible that their fracture strengths are lower than those along the $\langle 111 \rangle$ direction. The Si NWs tested in our experiments possess much larger fracture strength than Si thin films (1–4 GPa)⁴⁶ and NWs with larger diameters (0.03–4 GPa).^{21,28} A similar fracture strength of 12 GPa in VLS-grown Si NWs have been reported recently using the AFM bending technique, but their NW diameters ranged between 100 and 200 nm.³ The size effects on the fracture strain and strength are assumed to be related to the defects presented in the NWs. For NWs with smaller size, the possibility of defects in the material is reduced, leading to the increase of the fracture strain and strength. This is a common phenomenon in nanoscale systems.

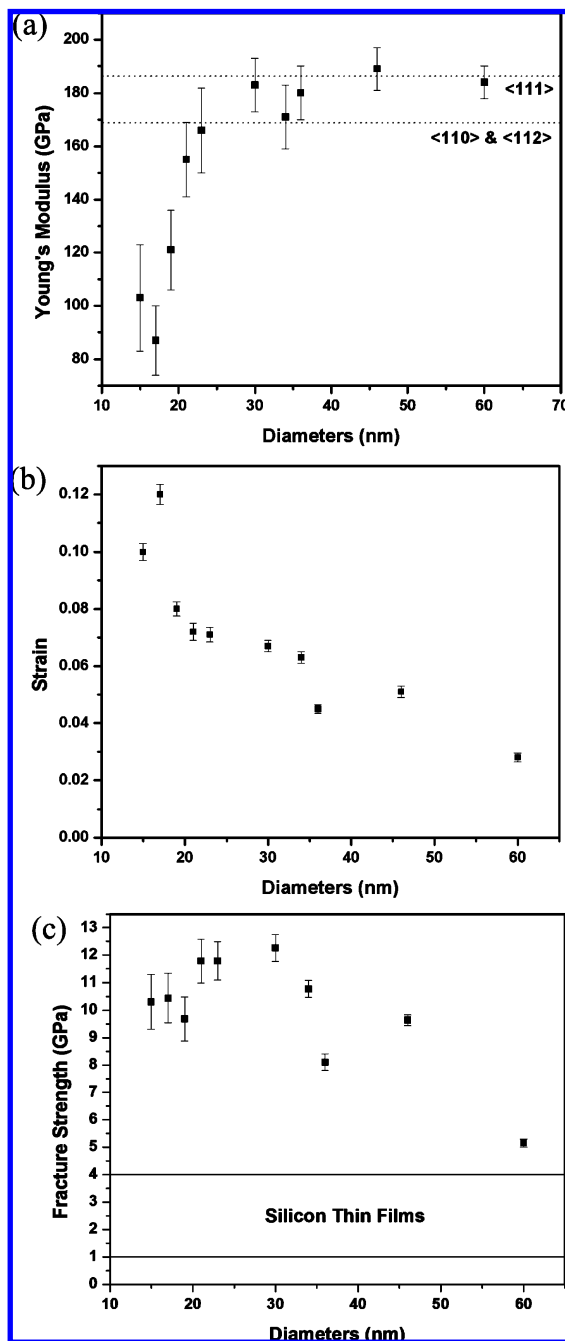


Figure 4. Plots of the (a) Young's modulus, (b) fracture strain, and (c) fracture strength vs diameters of the NWs from the tension tests.

The relation between the fracture strength and the side surface area of the Si NWs was also investigated, as shown in Figure 5. The mean fracture strengths from some Si thin films⁴⁶ and NWs^{3,24,28} are summarized in the same figure as well. It can be found that the fracture strength is sensitive to the side surface area despite the difference in fabricating the thin films and NWs. The strength increases with decreasing side surface area, which confirms that the defects on surface of the thin films and NWs play an important role in causing the fracture. Interestingly, with the decrease of the side surface area, the increase rate of the fracture strength for the NWs in our work is found to be much higher than that for the thin films. It is plausible that Si NWs synthesized by

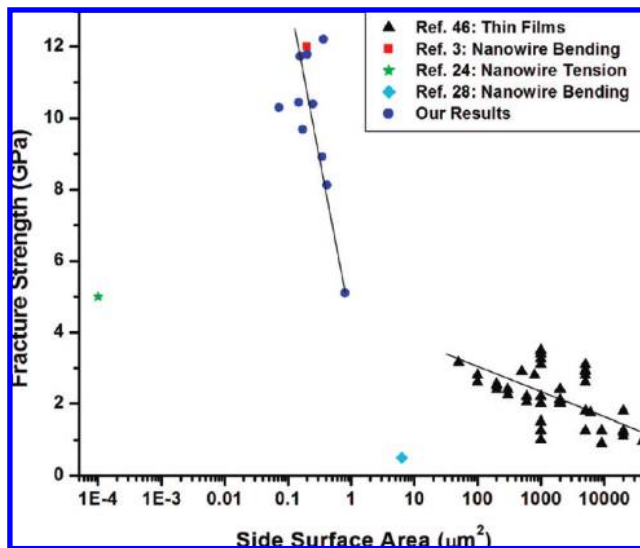


Figure 5. Plot of fracture strength vs the side surface area of the Si NWs and thin films. The fitted lines of our results and the thin films results show different slope, which might be related to the surface quality associated with two different manufacturing methods. Si NWs in refs 3 and 28 and our results are synthesized by the VLS method, while the Si NW in ref 24 was produced using a very different method, namely, nanometer-tip contact and retraction.

the VLS method possess fewer surface defects, thus better surface quality, compared to thin films fabricated using wet or dry etching methods.

The brittle fracture observed in all our experiments is in contrary to a recent report by Han et al.,² where large-strain plasticity was observed for Si NWs with diameters smaller than 60 nm under tension in TEM. The authors found that the tensile plasticity was initiated by the emergence of a high density of dislocations followed by the development of a continuous disordered lattice by the emission of dislocations. It should be noted that the most unambiguous method for assessing plasticity is loading–unloading in tensile tests. If there is a plastic strain, it remains when the material is totally unloaded. Unfortunately, Han's experiments do not possess the capability for stress measurement and thus cannot quantitatively assess the loading–unloading behavior. Two possible reasons can be suggested to explain the discrepancy between the two experimental results: effects of high-energy electron beam and difference in NW preparation. First of all, the electron beam irradiation in TEM is much stronger than that in SEM. The high-energy electron beam can increase the temperature of the NW. It can also significantly enhance diffusion and dislocation mobility, which both may contribute to the observed ductility.³³ A recent in situ TEM study on NaCl NWs also observed superplastic deformation, and the authors confirmed that electron beam irradiation enhanced ductility.⁴⁷ Another example on the superplasticity comes from carbon nanotubes (CNTs). In situ TEM tension experiments showed that, at high temperatures, individual single-walled CNTs can undergo superplastic deformation (becoming nearly 280% longer than its original length, much larger than the theoretical strain of CNTs at room temperature).⁴⁸ Dramatically enhanced atomic diffusion was also

observed for multiwalled CNTs under in situ TEM.⁴⁹ Second, the Si NWs in our experiments were synthesized using the CVD-VLS method,³⁴ while those in Han's experiments were synthesized using the thermal evaporation method. Furthermore, the NWs in Han's experiments were processed in hydrofluoric acid, which might cause an adverse effect on the NW properties. Similar BDT of Si NWs was observed in MD simulations by Kang and Cai.³³ They found that NWs with diameters less than 4 nm become ductile at room temperature, while thicker NWs become ductile only at elevated temperatures. In our experiments, no plasticity was observed for the Si NW with diameter as small as 15 nm at room temperature, which is in line with the MD simulations.

In summary, the Young's modulus and fracture strength of Si NWs with diameters between 15 and 60 nm and lengths between 1.5 and 4.3 μm were measured. The NWs, grown by the VLS process, were subjected to in situ tensile tests inside a SEM. The Young's modulus of Si NWs was found to be close to the bulk value (187 GPa for $\langle 111 \rangle$ orientation) when the diameters are larger than 30 nm. However, the softening trend is obvious when the diameters of the NW are smaller than 30 nm; the Young's modulus of the NWs decreases with the decreasing diameters. Our experiments also showed that fracture strain and strength of Si NWs increased as the NW diameter decreased. The maximum strength was found to be over 12 GPa. The fracture strength also increased with the decrease of the side surface area; the increase rate for the chemically synthesized Si NWs was found to be much higher than that for the microfabricated Si thin films. Repeated loading and unloading during tensile tests demonstrated that the NWs are linear elastic until fracture without appreciable plasticity.

Acknowledgment. This work was supported by the National Science Foundation under Award No. CMMI-0826341 and the Faculty Research and Professional Development Fund from North Carolina State University. The authors would like to thank Letian Lin and Professor Lu-Chang Qin at UNC—Chapel Hill for taking TEM images of the Si NWs and Professor Harold Park at University of Colorado for valuable discussions.

Supporting Information Available: High-resolution TEM image of a Si NW and SEM images of a Si NW before and after tension testing. This material is available free of charge via the Internet at <http://pubs.acs.org>.

References

- (1) Lu, W.; Lieber, C. M. *J. Phys. D: Appl. Phys.* **2006**, *39*, R387.
- (2) Han, X.; Zheng, K.; Zhang, Y.; Zhang, X.; Zhang, Z.; Wang, Z. L. *Adv. Mater.* **2007**, *19*, 2112.
- (3) Hoffmann, S.; Utke, I.; Moser, B.; Michler, J.; Christiansen, S. H.; Schmidt, V.; Senz, S.; Werner, P.; Gosele, U.; Ballif, C. *Nano Lett.* **2006**, *6*, 622.
- (4) Cui, Y.; Duan, X.; Hu, J.; Lieber, C. M. *J. Phys. Chem. B* **2000**, *104*, 5213.
- (5) Holmes, J. D.; Johnston, K. P.; Doty, R. C.; Korgel, B. A. *Science* **2000**, *287*, 1471.
- (6) He, R. R.; Yang, P. D. *Nat. Nanotechnol.* **2006**, *1*, 42.
- (7) Hochbaum, A. I.; Chen, R.; Delgado, R. D.; Liang, W.; Garnett, E. C.; Najarian, M.; Majumdar, A.; Yang, P. *Nature* **2008**, *451*, 163.
- (8) Boukai, A. I.; Bunimovich, Y.; Tahir-Kheli, J.; Yu, J.-K., III; W. A. G.; Heath, J. R. *Nature* **2008**, *451*, 168.

- (9) Li, D.; Wu, Y.; Kim, P.; Shi, L.; Yang, P.; Majumdar, A. *Appl. Phys. Lett.* **2003**, *83*, 2934.
- (10) Cui, Y.; Lieber, C. M. *Science* **2001**, *291*, 851.
- (11) Goldberger, J.; Hochbaum, A. I.; Fan, R.; Yang, P. *Nano Lett.* **2006**, *6*, 973.
- (12) Xiang, J.; Lu, W.; Hu, Y. J.; Yan, H.; Lieber, C. M. *Nature* **2006**, *441*, 489.
- (13) Patolsky, F.; Lieber, C. M. *Mater. Today* **2005**, *8*, 20.
- (14) Feng, X. L.; He, R.; Yang, P.; Roukes, M. L. *Nano Lett.* **2007**, *7*, 1953.
- (15) Huang, Y.; Duan, X.; Lieber, C. M. *Small* **2005**, *1*, 142.
- (16) Li, X.; Ono, T.; Wang, Y.; Esashi, M. *Appl. Phys. Lett.* **2003**, *83*, 3081.
- (17) Bai, X. D.; Gao, P. X.; Wang, Z. L.; Wang, E. G. *Appl. Phys. Lett.* **2003**, *82*, 4806.
- (18) Chen, C. Q.; Shi, Y.; Zhang, Y. S.; Zhu, J.; Yan, Y. J. *Phys. Rev. Lett.* **2006**, *96*, 075505.
- (19) Jing, G. Y.; Duan, H. L.; Sun, X. M.; Zhang, Z. S.; Xu, J.; Li, D.; Wang, J. X.; Yu, D. P. *Phys. Rev. B* **2006**, *73*, 35409.
- (20) Heidelberg, A.; Ngo, L. T.; Wu, B.; Phillips, M. A.; Sharma, S.; Kamins, T. I.; Sader, J. E.; Boland, J. J. *Nano Lett.* **2006**, *6*, 1101.
- (21) Gordon, M. J.; Baron, T.; Dhalluin, F.; Gentile, P.; Ferret, P. *Nano Lett.* **2009**, *9*, 525.
- (22) Agrawal, R.; Peng, B.; Gdoutos, E.; Espinosa, H. D. *Nano Lett.* **2008**, *8*, 3668.
- (23) Desai, A. V.; Haque, M. A. *Sens. Actuators, A* **2007**, *134*, 169.
- (24) Kizuka, T.; Takatani, Y.; Asaka, K.; Yoshizaki, R. *Phys. Rev. B* **2005**, *72*, 035333.
- (25) Zhu, Y.; Moldovan, N.; Espinosa, H. D. *Appl. Phys. Lett.* **2005**, *86*, 013506.
- (26) Ding, W.; Eitan, A.; Fisher, F. T.; Chen, X.; Dikin, D.; Andrews, R.; Brinson, L. C.; Schadler, L. S.; Ruoff, R. S. *Nano Lett.* **2003**, *3*, 1593.
- (27) Li, X.; Gao, H.; Murphy, C. J.; Caswell, K. K. *Nano Lett.* **2003**, *3*, 1495.
- (28) Tabib-Azar, M.; Nassirou, M.; Wang, R.; Sharma, S.; Kamins, T. I.; Islam, M. S.; Williams, R. S. *Appl. Phys. Lett.* **2005**, *87*, 113102.
- (29) Park, H. S.; Cai, W.; D., H.; Espinosa, H. D.; Huang, H. *MRS Bull.* **2009**, *34*, 178.
- (30) Lee, B.; Rudd, R. E. *Phys. Rev. B* **2007**, *75*, 195328.
- (31) Kang, K.; Cai, W. *Philos. Mag.* **2007**, *87*, 2169.
- (32) Shim, H. W.; Zhou, L. G.; Huang, H.; Cale, T. S. *Appl. Phys. Lett.* **2005**, *86*, 151912.
- (33) Kang, K.; Cai, W. *J. Mech. Phys. Solids* **2008**, submitted.
- (34) Wu, Y.; Cui, Y.; Huynh, L.; Barrelet, C. J.; Bell, D. C.; Lieber, C. M. *Nano Lett.* **2004**, *4*, 433.
- (35) Ma, D. D. D.; Lee, C. S.; Au, F. C. K.; Tong, S. Y.; Lee, S. T. *Science* **2003**, *299*, 1874.
- (36) Zhu, Y.; Espinosa, H. D. *Proc. Natl. Acad. Sci. U.S.A.* **2005**, *102*, 14503.
- (37) Yu, M. F.; Louire, O.; Dyer, M. J.; Moloni, K.; Kelly, T. F.; Ruoff, R. S. *Science* **2000**, *287*, 637.
- (38) Sader, J. E.; Chon, J. W. M.; Mulvaney, P. *Rev. Sci. Instrum.* **1999**, *70*, 3967.
- (39) Courtney, T. H. *Mechanical Behavior of Materials*; McGraw-Hill: Boston, 2000, ISBN 0070285942.
- (40) Miller, R. E.; Shenoy, V. B. *Nanotechnology* **2000**, *11*, 139.
- (41) Shim, H. W.; Zhou, L. G.; Huang, H.; Cale, T. S. *Appl. Phys. Lett.* **2005**, *86*, 151912.
- (42) Park, H. S. *J. Appl. Phys.* **2008**, *103*, 123504.
- (43) Liang, H. Y.; Upmanyu, M.; Huang, H. C. *Phys. Rev. B* **2005**, *71*, 241403.
- (44) Sadeghian, H.; Yang, C. K.; Goosen, J. F. L.; Drift, E. V. D.; Bossche, A.; French, P. J.; Keulen, F. V. *Appl. Phys. Lett.* **2009**, *94*, 221930.
- (45) Kelly, A.; Macmillan, N. H. *Strong Solids*; Monographs on the Physics and Chemistry of Materials; Clarendon Press: Oxford, 1986, ISBN 0-19-851362-3.
- (46) Tsuchiya, T.; Hirata, M.; Chiba, N.; Udo, R.; Yoshitomi, Y.; Ando, T.; Sato, K.; Takashima, K.; Higo, Y.; Saotome, Y.; Ogawa, H.; Ozaki, K. *Microelectromech. Syst.* **2005**, *14*, 1178.
- (47) Moore, N. W.; Luo, J. H.; Huang, J. Y.; Mao, S. X.; Houston, J. E. *Nano Lett.* **2009**, *9*, 2295.
- (48) Huang, J. Y.; Chen, S.; Wang, Z. Q.; Kempa, K.; Wang, Y. M.; Jo, S. H.; Chen, G.; Dresselhaus, M. S.; Ren, Z. F. *Nature* **2006**, *439*, 281.
- (49) Banhart, F.; Li, J. X.; Krasheninnikov, A. V. *Phys. Rev. B* **2005**, *71*, 241408.

NL902132W